Electroexcitation of nucleon resonances of the [70,1^{−}] multiplet in a light-front relativistic quark model

I. G. Aznauryan and V. D. Burkert

Electroexcitation of nucleon resonances of the $[70, 1^-]$ multiplet in a light-front relativistic quark model

I.G. Aznauryan[1, 2] and V.D. Burkert[1]

[1] *Thomas Jefferson National Accelerator Facility, Newport News, Virginia 23606, USA*
[2] *Yerevan Physics Institute, 375036 Yerevan, Armenia*
(Dated: May 19, 2017)

We utilize the light-front relativistic quark model to predict the $3q$ core contribution to the electroexcitation of nucleon resonances of the $[70, 1^-]$ multiplet on the proton and neutron at $Q^2 < 5$ GeV^2. The investigation is motivated by new experimental data from CLAS on meson electroproduction in a wide range of the hadronic invariant mass including the full third nucleon resonance region up to $\sqrt{s} = 1.8$ GeV. For the states $N(1520)\frac{3}{2}^-$, $N(1535)\frac{1}{2}^-$, and $N(1675)\frac{5}{2}^-$, experimental results on the electroexcitation amplitudes on the proton are available in a wide range of Q^2. This allowed us also to quantify the expected meson-baryon contributions to these amplitudes as a function of Q^2.

I. INTRODUCTION

Experiments on the new generation of electron beam facilities have led to dramatic progress in the investigation of the electroexcitation of nucleon resonances, and a significant role in the interpretation of new data is played by quark models, in particular, the light-front relativistic quark model (LF RQM).

Measurements with the CLAS detector at Jefferson Lab, for the first time, have enabled the determination of the electroexcitation amplitudes of the Roper resonance $N(1440)\frac{1}{2}^+$ on the proton in a range of the photon virtuality Q^2 up to 4.5 GeV^2 [1]. The comparison of these results with the LF RQM predictions [2, 3] was crucial for the identification of the $N(1440)\frac{1}{2}^+$ as a predominantly radial excitation of the three-quark ($3q$) ground state, with additional non-3-quark contributions needed to describe the low Q^2 behavior of the amplitudes.

The $\gamma^* p \to \Delta(1232)\frac{3}{2}^+$ transition amplitudes have been measured in an even wider range of Q^2 (0.06 ÷ 8 GeV^2) [1, 4–10]. The obtained data confirm the meson-cloud contribution as a source of the long-standing descreapancy between the data and quark model predictions for the magnetic-dipole form factor of this transition, and the 'bare' contribution to this form factor, found within dynamical reaction model [11–13], is very close to the LF RQM predictions [14–16]. At $Q^2 > 2$ GeV^2, the LF RQM [15] also reproduces the small ratio R_{EM} of electric and magnetic amplitudes and the sharply growing ratio of scalar to magnetic amplitudes R_{SM} for this transition, including its sign.

An important conclusion could be drawn from the results on the $\gamma^* p \to N(1675)\frac{5}{2}^-$ amplitudes extracted from CLAS data [17]. A special feature of the $N(1675)\frac{5}{2}^-$ state is the strong suppression of its transverse helicity amplitudes through excitations of the quark core from the proton. The data show significantly more strength at the real photon point and at moderately high Q^2 than

what is predicted from various constituent quark models. This feature allowed one to draw conclusion regarding the dominant strength of the meson-baryon contribution to the $\gamma^* p \to N(1675)\frac{5}{2}^-$ transverse helicity amplitudes [18], which is supported by the results of the dynamical coupled-channels approach [13].

Meson electroproduction experiments have been performed mostly on hydrogen targets and have allowed for the extraction of the electroexcitation amplitudes for the $\Delta(1232)\frac{3}{2}^+$ [1, 4–10] employing the $\gamma^* p \to p\pi^0$ channel, and the $N(1535)\frac{1}{2}^-$ [1, 19–22] using both the $\gamma^* p \to p\eta$ and $\gamma^* p \to n\pi^+$ channels, covering the range of Q^2 up to 8 GeV^2. For the $N(1440)\frac{1}{2}^+$, $N(1520)\frac{3}{2}^-$, $N(1675)\frac{5}{2}^-$, $N(1680)\frac{5}{2}^+$, and $N(1710)\frac{1}{2}^+$, the helicity amplitudes have been extracted for $Q^2 < 4.5$ GeV^2 employing both the $\gamma^* p \to n\pi^+$ and $\gamma^* p \to p\pi^+\pi^-$ channels [1, 17, 23–25], and for the states $\Delta(1620)\frac{1}{2}^-$, $N(1650)\frac{1}{2}^-$, $\Delta(1700)\frac{3}{2}^-$, and $N(1720)\frac{3}{2}^+$, electrocouplings have been determined in the range $Q^2 = 0.65 \div 1.3$ GeV^2 [23–25] using the $\gamma^* p \to p\pi^+\pi^-$ reaction. Currently new data are in preparation by the CLAS Collaboration for the $ep \to ep\pi^0$ process in the same kinematics region as the CLAS data in the $ep \to en\pi^+$ channel [17, 26]. The two-channel analysis will allow for the extraction of all resonances in the third nucleon resonance region at $Q^2 < 4.5$ GeV^2. Other analyses, such as for the processes $en(p_s) \to ep\pi^-(p_s)$ on a deuterium target and $ep \to ep\pi^+\pi^-$ are also in preparation.

Therefore, in the near future the CLAS experiment will provide us with rich information on the electroexcitation of the nucleon resonances from the multiplet $[70, 1^-]$ at $Q^2 < 4.5$ GeV^2, and our goal in the present investigation is to extend our previous results on the $N(1520)\frac{3}{2}^-$ and $N(1535)\frac{1}{2}^-$ within the LF RQM [27] by comprehensive investigation of electroexcitation of all resonances assigned to the $[70, 1^-]$-plet on the proton and neutron

We use an approach based on the LF dynamics that

presents the most suitable framework for describing the transitions between relativistic bound systems [28–30]. In early works by Berestetsky and Terent'ev [29], the approach was based on the construction of the generators of the Poincaré group in the LF. It was later formulated in the infinite momentum frame (IMF) [31, 32]. This demonstrated more clearly that for longitudinal components of the electromagnetic current $J_{em}^{0,z}$, diagrams violating the impulse approximation, i.e. diagrams containing vertices like $\gamma^* \to q\bar{q}$, do not contribute. The interpretation of the results for the $\gamma^* N \to N(N^*)$ transitions in terms of the vertices $N(N^*) \leftrightarrow 3q$ and the corresponding wave functions became more evident. A similar approach was developed and used in the investigation of electroexcitation of nucleon resonances in Ref. [2] within LF Hamiltonian dynamics [33]. Both approaches use a complete set of orthogonal wave functions that correspond to the classification of the nucleon and nucleon resonances within the group $SU(6) \times O(3)$ in the c.m.s. of the constituent quarks. It was shown in Ref. [32] that the wave functions of the system of quarks in the IMF and in their c.m.s. are related through Melosh rotations of quark spin matrices [34]. The same result was obtained in Ref. [2] within LF Hamiltonian dynamics.

This paper is organized as follows. In Section II we present the LF RQM formalism to compute the $\gamma^* N \to N^*$ transition amplitudes. We specify the IMF where the LF RQM is built and the relations between the $< N^* | J_{em}^\mu | N >$ matrix elements and the $N(N^*) \leftrightarrow 3q$ wave functions in this frame. Furthermore, the relations between these matrix elements and the $\gamma^* N \to N^*$ form factors and transition helicity amplitudes are presented. In Section III we discuss the mixings of the states $N(1535)\frac{1}{2}^- / N(1650)\frac{1}{2}^-$ and $N(1520)\frac{3}{2}^- / N(1700)\frac{3}{2}^-$ and present the available information on the corresponding mixing angles. The results are presented in Section IV and further discussed and summarized in Section V.

II. THE $\gamma^* N \to N^*$ TRANSITION AMPLITUDES IN THE LF RQM

The $\gamma^* N \to N^*$ transition amplitudes have been evaluated within the approach of Ref. [32] where the LF RQM is formulated in the infinite momentum frame chosen in such a way that the initial hadron moves along the z-axis with momentum $P \to \infty$, the virtual photon momentum is $k^\mu = \left(\frac{M^2 - m^2 - \mathbf{Q}_\perp^2}{4P}, \mathbf{Q}_\perp, -\frac{M^2 - m^2 - \mathbf{Q}_\perp^2}{4P} \right)$, the final hadron momentum is $P' = P + k$, and $Q^2 \equiv -k^2 = \mathbf{Q}_\perp^2$; m and M are the masses of the nucleon and resonance, respectively. In this frame, the matrix elements of the electromagnetic current for the $\gamma^* N \to N^*$ transition have the form:

$$< N^*, S_z' | J_{em}^\mu | N, S_z > |_{P \to \infty}$$
$$= 3eQ_a \int \Psi'^+(p_a', p_b', p_c') \Gamma_a^\mu \Psi(p_a, p_b, p_c) d\Gamma, \quad (1)$$

where S_z and S_z' are the projections of the hadron spins in the z-direction. In (1), it is supposed that the photon interacts with quark a (the quarks in the hadrons are denoted by a, b, c), Q_a is the charge of this quark in units of e ($e^2/4\pi = 1/137$); Ψ and Ψ' are wave functions in the vertices $N(N^*) \leftrightarrow 3q$; p_i and p_i' ($i = a, b, c$) are the quark momenta in the IMF; $d\Gamma$ is the phase space volume; Γ_a^μ corresponds to the vertex of the quark interaction with the photon:

$$x_a \Gamma_a^x = 2p_{ax} + Q_x + iQ_y \sigma_z^{(a)}, \quad (2)$$

$$x_a \Gamma_a^y = 2p_{ay} + Q_y - iQ_x \sigma_z^{(a)}, \quad (3)$$

$$\Gamma_a^0 = \Gamma_a^z = 2P, \quad (4)$$

where x_i ($i = a, b, c$) is the fraction of the initial hadron momentum carried by the quark:

$$\mathbf{p}_i = x_i \mathbf{P} + \mathbf{q}_{i\perp}, \quad \sum_i \mathbf{q}_{i\perp} = 0, \quad \sum_i x_i = 1. \quad (5)$$

The invariant mass of the system of initial quarks has the form:

$$M_0^2 = \left(\sum_i p_i \right)^2 = \sum_i \frac{\mathbf{q}_{i\perp}^2 + m_q^2}{x_i}, \quad (6)$$

where m_q is the quark mass.

We define the c.m.s. of the initial quarks with the quark three-momenta $\mathbf{q}_i$ ($i = a, b, c$), where the quark transverse momenta are given by (5), and the z-components are defined as:

$$q_{iz} + \omega_i = M_0 x_i, \quad \omega_i = \sqrt{m_q^2 + \mathbf{q}_i^2}, \quad (7)$$

$$q_{iz} = \frac{1}{2} \left(x_i M_0 - \frac{m_q^2 + \mathbf{q}_{i\perp}^2}{x_i M_0} \right), \quad (8)$$

$$M_0 = \sum_i \omega_i, \quad \sum_i \mathbf{q}_i = 0. \quad (9)$$

For the final state quarks, the quantities defined by (5-9) are expressed through $\mathbf{P}'$, p_i', $\mathbf{q}_i'$, and M_0'.

According to results of Ref. [32], the wave function Ψ in (1) is related to the wave function in the c.m.s. of quarks defined according to (5-9) through Melosh matrices [34]:

$$\Psi = U^+(p_a) U^+(p_b) U^+(p_c) \Psi_{fss} \Phi(\mathbf{q}_a, \mathbf{q}_b, \mathbf{q}_c). \quad (10)$$

Here we have separated the flavor-spin-space (Ψ_{fss}) and the spatial (Φ) parts of the c.m.s. wave function. The Melosh matrices are

$$U(p_i) = \frac{m_q + M_0 x_i + i\epsilon_{lm} \sigma_l q_{im}}{\sqrt{(m_q + M_0 x_i)^2 + \mathbf{q}_{i\perp}^2}}. \quad (11)$$

We construct the flavor-spin-space parts of the wave functions in the c.m.s. of the quarks by utilizing the rules [2, 35] that correspond to the classification of the nucleon and nucleon resonances within the group $SU(6) \times O(3)$.

The phase space volume in (1) has the form:

$$d\Gamma = \frac{1}{(2\pi)^6} \frac{d\mathbf{q}_{b\perp} d\mathbf{q}_{c\perp} dx_b dx_c}{4x_a x_b x_c}. \quad (12)$$

A. The relations between matrix elements of (1) and the $\gamma^* N \to N^*$ transition helicity amplitudes

Electroexcitation of the states with $J^P = \frac{1}{2}^-$ and $J^P = \frac{3}{2}^-, \frac{5}{2}^-$ that enter the multiplet $[70, 1^-]$ is described, respectively, by two and three form factors, which we define according to Refs. [36, 37] in the following way:

$$< N^*(\tfrac{1}{2}^-)|J_{em}^\mu|N > \equiv e\bar{u}(P')\gamma_5 \tilde{J}^\mu u(P), \quad (13)$$

$$< N^*(\tfrac{3}{2}^-)|J_{em}^\mu|N > \equiv e\bar{u}_\nu(P')\Gamma^{\nu\mu} u(P), \quad (14)$$

$$< N^*(\tfrac{5}{2}^-)|J_{em}^\mu|N > \equiv e\bar{u}_{\nu\nu_1}(P')k^{\nu_1}\gamma_5\Gamma^{\nu\mu} u(P), \quad (15)$$

where

$$\tilde{J}^\mu = \left(\not{k}k^\mu - k^2\gamma^\mu\right)G_1 + [\not{k}\mathcal{P}^\mu - (\mathcal{P}k)\gamma^\mu]G_2, \quad (16)$$

$$\Gamma^{\nu\mu}(Q^2) = G_1\mathcal{H}_1^{\nu\mu} + G_2\mathcal{H}_2^{\nu\mu} + G_3\mathcal{H}_3^{\nu\mu}, \quad (17)$$

$$\mathcal{H}_1^{\nu\mu} = \not{k}g^{\nu\mu} - k^\nu\gamma^\mu, \quad (18)$$

$$\mathcal{H}_2^{\nu\mu} = k^\nu P'^\mu - (kP')g^{\nu\mu}, \quad (19)$$

$$\mathcal{H}_3^{\nu\mu} = k^\nu k^\mu - k^2 g^{\nu\mu}. \quad (20)$$

Here $\mathcal{P} \equiv \frac{1}{2}(P' + P)$, $u(P), u(P')$ are the Dirac spinors and $u_\nu(P')$, $u_{\nu\nu_1}(P')$ are the generalized Rarita-Schwinger spinors.

In the LF RQM under consideration, the form factors $G_i(Q^2)$ are derived through the matrix elements (1). For the $J^P = \frac{1}{2}^-$ resonances, the relations between the form factors and the matrix elements (1) are following:

$$\frac{1}{2P} < N^*, \tfrac{1}{2}|J_{em}^{0,z}|N, \tfrac{1}{2} > |_{P\to\infty} = Q^2 G_1(Q^2), (21)$$

$$\frac{1}{2P} < N^*, \tfrac{1}{2}|J_{em}^{0,z}|N, -\tfrac{1}{2} > |_{P\to\infty} =$$
$$= -\frac{M+m}{2}QG_2(Q^2). \quad (22)$$

For the $J^P = \frac{3}{2}^-$ resonances, these relations are:

$$\frac{1}{2P} < N^*, \tfrac{3}{2}|J_{em}^{0,z}|N, \tfrac{1}{2} > |_{P\to\infty} =$$
$$-\frac{Q}{\sqrt{2}}\left[G_1(Q^2) - \frac{M+m}{2}G_2(Q^2)\right], \quad (23)$$

$$\frac{1}{2P} < N^*, \tfrac{3}{2}|J_{em}^{0,z}|N, -\tfrac{1}{2} > |_{P\to\infty} = \frac{Q^2}{2\sqrt{2}}G_2(Q^2), (24)$$

$$< N^*, \tfrac{3}{2}|J_{em}^x + iJ_{em}^y|N, -\tfrac{1}{2} > |_{P\to\infty} = \frac{Q^3}{\sqrt{2}}G_3(Q^2), (25)$$

and for the $J^P = \frac{5}{2}^-$ resonances, we have:

$$\frac{1}{2P} < N^*, \tfrac{5}{2}|J_{em}^{0,z}|N, \tfrac{1}{2} > |_{P\to\infty} =$$
$$-Q^2\left[G_1(Q^2) + \frac{M-m}{2}G_2(Q^2)\right], \quad (26)$$

$$\frac{1}{2P} < N^*, \tfrac{5}{2}|J_{em}^{0,z}|N, -\tfrac{1}{2} > |_{P\to\infty} = -\frac{Q^3}{2}G_2(Q^2), (27)$$

$$< N^*, \tfrac{5}{2}|J_{em}^x + iJ_{em}^y|N, -\tfrac{1}{2} > |_{P\to\infty} = Q^4 G_3(Q^2). (28)$$

The relations between the $\gamma^* N \to N^*\frac{1}{2}^-$ helicity amplitudes and the form factors $G_1(Q^2), G_2(Q^2)$ are as follows:

$$A_{\frac{1}{2}} = b\left[2Q^2 G_1 - (M^2 - m^2)G_2\right], \quad (29)$$

$$S_{\frac{1}{2}} = -b\frac{K}{\sqrt{2}}[2(M-m)G_1 + (M+m)G_2], \quad (30)$$

$$b \equiv e\sqrt{\frac{Q_+}{8m(M^2 - m^2)}}, \quad (31)$$

$$K \equiv \frac{\sqrt{Q_+ Q_-}}{2M}, \quad (32)$$

$$Q_\pm \equiv (M \pm m)^2 + Q^2. \quad (33)$$

For the resonances with $J^P = \frac{3}{2}^-$ and $\frac{5}{2}^-$ we have:

$$A_{1/2} = h_3 X, \quad A_{3/2} = \mp\sqrt{3}h_2 X, \quad (34)$$

$$S_{1/2} = \mp h_1 \frac{K}{\sqrt{2}M}X, \quad (35)$$

$$X \equiv K^{l-1}e\sqrt{\frac{Q_\pm}{32Jm(M^2 - m^2)}}, \quad l = J - \frac{1}{2}, \quad (36)$$

where

$$h_1(Q^2) = \mp 4MG_1(Q^2) + 4M^2 G_2(Q^2) +$$
$$2(M^2 - m^2 - Q^2)G_3(Q^2), \quad (37)$$

$$h_2(Q^2) = -2(\mp M + m)G_1(Q^2) -$$
$$(M^2 - m^2 - Q^2)G_2(Q^2) + 2Q^2 G_3(Q^2), \quad (38)$$

$$h_3(Q^2) = \pm\frac{2}{M}[Q^2 + m(\mp M + m)]G_1(Q^2) +$$
$$(M^2 - m^2 - Q^2)G_2(Q^2) - 2Q^2 G_3(Q^2), \quad (39)$$

and the upper and lower signs correspond, respectively, to $J^P = \frac{3}{2}^-$ and $\frac{5}{2}^-$ resonances.

III. MIXING OF $N(1535)\frac{1}{2}^-$ / $N(1650)\frac{1}{2}^-$ AND $N(1520)\frac{3}{2}^-$ / $N(1700)\frac{3}{2}^-$

The multiplet $[70, 1^-]$ consists of the following states: $N\frac{1}{2}^-(^28_{1/2})$, $N\frac{3}{2}^-(^28_{3/2})$, $N\frac{1}{2}^-(^48_{1/2})$, $N\frac{3}{2}^-(^48_{3/2})$, $N\frac{5}{2}^-(^48_{5/2})$, $\Delta\frac{1}{2}^-(^210_{1/2})$, and $\Delta\frac{3}{2}^-(^210_{3/2})$, where we

use the notation $^{2S+1}SU(3)_J$, which gives the assignment of the state according to the $SU(3)$ group, S is the total spin of the quarks and J is the spin of the resonance. The resonances with $J^P = \frac{1}{2}^-$ and $\frac{3}{2}^-$ can be composed, respectively, from the states $^2 8_{1/2}$, $^4 8_{1/2}$ and $^2 8_{3/2}$, $^4 8_{3/2}$, and therefore can be mixings of these states:

$$N(1535)\tfrac{1}{2}^- = \cos\theta_S |^2 8_{1/2}> - \sin\theta_S |^4 8_{1/2}>, \quad (40)$$

$$N(1650)\tfrac{1}{2}^- = \sin\theta_S |^2 8_{1/2}> + \cos\theta_S |^4 8_{1/2}>, \quad (41)$$

$$N(1520)\tfrac{3}{2}^- = \cos\theta_D |^2 8_{3/2}> - \sin\theta_D |^4 8_{3/2}>, \quad (42)$$

$$N(1700)\tfrac{3}{2}^- = \sin\theta_D |^2 8_{3/2}> + \cos\theta_D |^4 8_{3/2}> . \quad (43)$$

There is information on the mixing angles θ_S and θ_D obtained from the description of the resonance masses within the quark model with QCD-inspired interquark forces [38] and from experimental data on the decay widths of the resonances in the πN channel [39]. The results of Ref. [39] are based on the relations:

$$< \pi N|^2 8_{1/2}> / < \pi N|^4 8_{1/2}> = -2, \quad (44)$$

$$< \pi N|^2 8_{3/2}> / < \pi N|^4 8_{3/2}> = 2\sqrt{10}, \quad (45)$$

that follow from the $SU(6)_W$ symmetry. The same relations have been obtained in Ref. [40] within the LF RQM by relating the $< \pi N|N^* >$ amplitudes to the matrix elements of the axial-vector current $< N^*|J_{ax}^\mu|N >$ using the hypothesis of partially conserved axial-vector current (PCAC) in the way suggested in Ref. [41]. The results of Ref. [39] are based on early data. Using recent data [42], we have revised the values of the mixing angles extracted from the πN widths of the resonances as:

$$\theta_S = -16.6 \pm 5°, \quad \theta_D = 11.5 \pm 4°, \quad (46)$$

instead of $\theta_S = -31.9°$ and $\theta_D = 10.4°$ in Ref. [39]. The large difference in θ_S is caused mainly by the significant change of the $N(1535)\frac{1}{2}^- \to \pi N$ width that resulted in an increase of the ratio of the mean values of the $N(1535)\frac{1}{2}^-$ and $N(1650)\frac{1}{2}^-$ πN decay widths from 0.3 to 0.8.

The mixing angles obtained from the description of the masses [38] are determined as:

$$\theta_S = -32°, \quad \theta_D = 6.3°. \quad (47)$$

IV. RESULTS

In this Section we present our results for the $3q$ core contribution to the helicity transition amplitudes for the electroexcitation of the resonances of the multiplet $[70, 1^-]$ on the proton and neutron (Figs. 1-12). The spatial part of the wave functions and parameters of the model have been specified in Ref. [27] via a description of the nucleon electromagnetic form factors by combining the $3q$ and pion-cloud contributions in the LF dynamics.

To study sensitivity to the form of the quark wave function, two forms of the spatial wave function have been employed in Ref. [27]:

$$\Phi_1 \sim \exp(-M_0^2/6\alpha_1^2), \quad (48)$$

$$\Phi_2 \sim \exp\left[-(\mathbf{q}_a^2 + \mathbf{q}_b^2 + \mathbf{q}_c^2)/2\alpha_2^2\right]. \quad (49)$$

A good description of the nucleon electromagnetic form factors up to $Q^2 = 16$ GeV^2 has been obtained with the nucleon taken in the form:

$$|N> = 0.95|3q> +0.313|\pi N>, \quad (50)$$

and with the wave functions (48,49) using the following oscillator parameters and parameterizations for the running quark mass as a function of Q^2:

$$\alpha_1 = 0.37 \text{ GeV}, \quad m_q^{(1)}(Q^2) = \frac{0.22 \text{ GeV}}{1 + Q^2/56 \text{ GeV}^2}, \quad (51)$$

$$\alpha_2 = 0.41 \text{ GeV}, \quad m_q^{(2)}(Q^2) = \frac{0.22 \text{ GeV}}{1 + Q^2/18 \text{ GeV}^2}. \quad (52)$$

For the resonances of the $[70, 1^-]$-plet, the results for the transition amplitudes obtained with the wave functions (48,49) and corresponding parameters (51,52) are very close to each other. The role of the running quark mass becomes visible above 3 GeV^2. At $Q^2 = 5$ GeV^2, it increases the transition helicity amplitudes by $25\%-35\%$ and $10\% - 15\%$ for the wave functions (48) and (49), respectively.

Meson electroproduction provides strong evidence that baryon resonances are not excited from quark transition alone, but that there can be significant contribution from meson-baryon interactions, including pion-loop contributions generated by nearly massless pions. A common feature of approaches that account for meson-baryon contributions is the more rapid drop of these contributions with increasing Q^2 compared to the $3q$ contributions. For the $N(1535)\frac{1}{2}^-$ and $N(1520)\frac{3}{2}^-$, it is expected that meson-baryon contributions can be neglected at $Q^2 > 2$ GeV^2 [13]. There are accurate data for the electroexcitation of these resonances on the proton, respectively, at $Q^2 < 8$ GeV^2 and 4.5 GeV^2. Therefore, we define the $3q$ contributions to the $N(1535)\frac{1}{2}^-$ and $N(1520)\frac{3}{2}^-$ resonances as:

$$|N^* > = c_{N^*}|3q> +..., \quad c_{N^*} < 1, \quad (53)$$

where we find the numerical values of c_{N^*} from the experimental transition helicity amplitudes, assuming they are dominated by the $3q$ contributions at $Q^2 > 2$ GeV^2. The weight factors c_{N^*} for the $N(1535)\frac{1}{2}^-$ and $N(1520)\frac{3}{2}^-$ are presented in the captions to Fig. 1 and Fig. 6.

A. Configuration mixings and the results for the $N(1535)\frac{1}{2}^-/N(1650)\frac{1}{2}^-$ and $N(1520)\frac{3}{2}^-/N(1700)\frac{3}{2}^-$

The results for the resonances $N(1535)\frac{1}{2}^-$, $N(1650)\frac{1}{2}^-$ and $N(1520)\frac{3}{2}^-$, $N(1700)\frac{3}{2}^-$ are shown in Figs. 1-4 and

6-9 taking into account the mixings discussed in Section III. It can be seen that the amplitudes for the resonances $N(1650)\frac{1}{2}^-$ and $N(1700)\frac{3}{2}^-$, taken as pure $^48_{1/2}$ and $^48_{3/2}$ states, are significantly smaller than the amplitudes for the $N(1535)\frac{1}{2}^-$ and $N(1520)\frac{3}{2}^-$. For this reason, the mixings play a significant role in the electroexcitation of the $N(1650)\frac{1}{2}^-$ and $N(1700)\frac{3}{2}^-$, and in Figs. 3, 4 and 8, 9, we present three kind of curves: thin solid curves for the unmixed states ($\theta_S = \theta_D = 0°$) and thick solid and dashed curves, respectively, for mixing angles from (46) and (47).

As the electroexcitation amplitudes for the states $^48_{1/2}$ and $^48_{3/2}$ are suppressed compared with the amplitudes for the states $^28_{1/2}$ and $^28_{3/2}$, the electroexcitation of the $N(1535)\frac{1}{2}^-$ and $N(1520)\frac{3}{2}^-$ is determined mainly by the first terms in (40,42). In addition, the predictions for the quark core contributions for these resonances in Figs. 1, 2 and 6, 7 contain weight factor c_{N^*} (see (53)), which we find from the experimental values of the transition helicity amplitudes on the proton, assuming that at $Q^2 > 2$ GeV^2 they are dominated by the $3q$ contributions. Therefore for the $N(1535)\frac{1}{2}^-$ and $N(1520)\frac{3}{2}^-$, different mixing angles from (46) and (47) result only in slightly different weight factors, while the predictions for the quark core contributions for different mixing angles coincide with each other.

It is known that the results for the $\gamma^*N \to N^*$ transition amplitudes extracted from experimental data contain an additional sign related to the vertex of the resonance coupling to the final state hadrons (see, for example, Ref. [36]). In the electroproduction of pions on nucleons this is the relative sign between the πNN^* and πNN vertices. For the resonances of the $[70, 1^-]$-plet, this sign has been found in Ref. [40] in the LF approach based on PCAC (see also Section III). In Ref. [40], the electroexcitation of the resonances of $[70, 1^-]$-plet on the proton and neutron has been investigated at $Q^2 = 0$, and the results for the transverse transition helicity amplitudes have been presented taking into account the relative sign between the πNN^* and πNN vertices. This sign is taken into account also in the results obtained in the present investigation and shown in Figs. 1-12. We mention that from the relations (40,41,44) it follows that in all considered cases of mixings, the relative sign between the $\pi NN(1535)$ and $\pi NN(1650)$ vertices is negative. This is important for understanding of the results for the $N(1650)\frac{1}{2}^-$.

B. SQTM and the results for the $N(1675)\frac{1}{2}^-$

We now comment on the results for the $N(1675)\frac{5}{2}^-$ shown in Figs. 11 and 12. The approximation of the single quark transition model (SQTM) [43–46] leads to selection rules, which for the resonances of the $[70, 1^-]$-plet, result in the suppression of the transition from the proton

to the states with $S = \frac{3}{2}$ for the transverse helicity amplitudes. These are the states $N\frac{1}{2}^-(^48_{1/2})$, $N\frac{3}{2}^-(^48_{3/2})$, and $N\frac{5}{2}^-(^48_{5/2})$. According to our results, relativistic effects violate this suppression weakly. For the $J = \frac{1}{2}$ and $\frac{3}{2}$ states, this can be seen from Figs. 3, 8, where the amplitudes for the electroexcitation of $N\frac{1}{2}^-(^48_{1/2})$ and $N\frac{3}{2}^-(^48_{3/2})$ are given by the thin solid lines. For the resonance $N(1675)\frac{5}{2}^-$, we also have a small violation of the suppression of the transverse helicity amplitudes for the electroexcitation on the proton (see Fig. 11). In contrast with the proton, the electroexcitation amplitudes on the neutron are large. In both cases, for the proton and neutron, similar predictions have been obtained in the quark model of Ref. [47].

C. Model uncertainties of the results for the $J^P = \frac{3}{2}^-$ and $\frac{5}{2}^-$ states

In Refs. [40, 48] it was shown that there are difficulties in the utilization of the LF approaches for hadrons with $J \geq 1$. In the approach of Refs. [29, 31, 32], these difficulties limit the number of form factors that can be found for the $J^P = \frac{3}{2}^-$ and $\frac{5}{2}^-$ states. According to Ref. [40], for electroexcitation of these states only those results are reliable that are based on utilization of (1) at $S'_z = J$ for the longitudinal components of the electromagnetic current $J^{0,z}_{em}$, i.e. the results for $G_1(Q^2)$ and $G_2(Q^2)$ obtained using (23,24) and (26,27). In our investigation, we complement these results by computing $G_3(Q^2)$ using the transverse component of the electromagnetic current $J^x_{em} + iJ^y_{em}$ ((25) and (28)). In Ref. [32] it is shown that the results based on the use of $J^x_{em} + iJ^y_{em}$ are less reliable, as the transition matrix elements in this case can contain contributions that violate the impulse approximation, namely, the contributions of diagrams containing vertices like $\gamma^* \to q\bar{q}$. For the resonances $N(1520)\frac{3}{2}^-$, $\Delta(1700)\frac{3}{2}^-$, and $N(1675)\frac{5}{2}^-$, we demonstrate in Figs. 6,7, 10,11,12, the uncertainties that can arise from the unknown contributions of $G_3(Q^2)$. We illustrate the possible size of the effect by setting $G_3(Q^2) = 0$. Strong effects are observed only for the longitudinal transition helicity amplitudes at $Q^2 < 1$ GeV^2. Similar uncertainties have been discussed in the LF RQM of Refs. [2, 48].

D. Inferred meson-baryon contributions

For the resonances $N(1520)\frac{3}{2}^-$, $N(1535)\frac{1}{2}^-$, and $N(1675)\frac{5}{2}^-$, data on electroexcitation amplitudes on the proton are available in a wide range of Q^2. This allowed us to quantify the expected meson-baryon contributions to these amplitudes at $Q^2 < 2 - 3$ GeV^2. The meson-baryon contributions inferred from the difference of the LF RQM predictions and the data are shown in Figs. 1,

Resonance	proton				neutron			
	$A_{1/2}$	$A_{3/2}$	$A_{1/2}$	$A_{3/2}$	$A_{1/2}$	$A_{3/2}$	$A_{1/2}$	$A_{3/2}$
	exp. [42]		exp $-$ LF RQM		exp. [42]		exp $-$ LF RQM	
$N(1520)\frac{3}{2}^-$	-20 ± 5	140 ± 10	-17 ± 5	-174 ± 10	-50 ± 10	-115 ± 10	25 ± 10	131 ± 10
$N(1535)\frac{1}{2}^-$	115 ± 15		-54 ± 15		-75 ± 20		102 ± 20	
$\Delta(1620)\frac{1}{2}^-$	40 ± 15		-152 ± 15					
$N(1675)\frac{5}{2}^-$	19 ± 8	20 ± 5	16 ± 8	15 ± 5	-60 ± 5	-85 ± 10	-13 ± 5	-23 ± 10
$\Delta(1700)\frac{3}{2}^-$	140 ± 30	140 ± 30	-85 ± 30	-59 ± 30				

TABLE I: Transverse transition helicity amplitudes at $Q^2 = 0$ for several states of the $[70, 1^-]$ multiplet for proton and neutron (in units of 10^{-3} GeV$^{-1/2}$). The first two columns show the RPP estimates [42]. Columns 3 and 4 show the inferred meson-baryon contributions obtained by subtracting the values obtained in the LF RQM and those from experimental data. The quoted uncertainties are from the experimental estimates.

6, 11 by the thin dashed-dotted lines. They correspond approximately to the mean values of the experimental data. The spread of these contributions can be deduced from the spread and uncertainties in the data.

The constituent quark contributions and the inferred meson-baryon contributions can be associated, respectively, with the bare and meson-cloud contributions in the dynamical coupled-channels approaches that incorporate the hadronic and electromagnetic channels. Much progress has been made recently within the EBAC/Argonne-Osaka coupled-channels analyses [13, 49, 50]. To date only preliminary results are available from the analyses that are based on the complete set of the CLAS pion electroproduction data in the entire Q^2 range up to 4.5 GeV^2 from the two channels $ep \rightarrow ep\pi^0$ and $ep \rightarrow en\pi^+$ [51, 52]. Results of the coupled-channels analyses are related to the resonance pole positions; with this in Refs. [13, 49] the absolute values of the meson cloud contributions continued to the real axis and evaluated at $W = 1.535$, 1.52, and 1.675 GeV were determined for $N(1520)\frac{3}{2}^-$, $N(1535)\frac{1}{2}^-$, and $N(1675)\frac{5}{2}^-$, respectively.

Most of the inferred meson-baryon contributions have a clear peak at $Q^2 = 0$, except for the $A_{1/2}(Q^2)$ amplitude of $N(1520)\frac{3}{2}^-$ and for the $S_{1/2}(Q^2)$ amplitude of $N(1535)\frac{1}{2}^-$. Such pronounced peaks are also characteristic for the meson cloud contributions in the coupled-channels analyses [13, 49, 51, 52]. Concerning the $A_{1/2}(Q^2)$ amplitude for the $N(1520)\frac{3}{2}^-$, we mention that in all coupled-channels analyses [13, 49, 51, 52] the results for the meson cloud contribution are by order of magnitude and Q^2 dependence very similar to our result.

For the states that are not affected by mixings, we present in Table I the inferred meson-baryon contributions to the transverse transition helicity amplitudes at the photon point $Q^2 = 0$. According to our results, the contributions for the $N(1520)\frac{3}{2}^-$, $N(1535)\frac{1}{2}^-$, and $N(1675)\frac{5}{2}^-$ are dominated by the isovector component.

V. SUMMARY AND DISCUSSION

In this work we presented results of a comprehensive investigation of electroexcitation of nucleon resonances belonging to the multiplet $[70, 1^-]$. The investigation was motivated by expected progress in the extraction of the electroexcitation amplitudes for these resonances from upcoming CLAS results on hydrogen and deuterium targets.

It is known that the three-quark structure of baryons resulted in predictions of a wealth of excited states with underlying spin-flavor and orbital symmetry of $SU(6) \times O(3)$. In spite of the essentially non-relativistic nature of this symmetry, it describes the observed quantum numbers and, in many cases, the masses of the resonances in the first, second, and third nucleon resonance regions. The LF dynamics is known as the most suitable framework for describing transitions of baryons composed of the relativistic constituent quarks. The important feature of the LF approach of Ref. [32], employed in the present investigation, as well of the LF approach of Ref. [2], is the fact that these approaches could solve in a uniform way the problem of the construction of an orthogonal set of wave functions for the relativistic quarks by preserving $SU(6) \times O(3)$ symmetry. This has been done by defining the symmetry in the c.m.s. of the constituent quarks defined by (5-9). Then it was shown that

in the IMF or LF framework, which are used for computing the transition amplitudes, the flavor-spin-space parts of wave functions are related to the wave functions in the c.m.s. of the quarks by the quark spin rotations given by the Melosh matrices. Therefore, in our calculations we employ the flavor-spin-space parts of the wave functions that in the c.m.s. of quarks correspond to the classification of states within the group $SU(6) \times O(3)$.

The pairs of resonances $N(1535)\frac{1}{2}^-$ / $N(1650)\frac{1}{2}^-$ and $N(1520)\frac{3}{2}^-$ / $N(1700)\frac{3}{2}^-$ with the same spin-parity can be composed, respectively, from the states $^28_{1/2}$ / $^48_{1/2}$ and $^28_{3/2}$ / $^48_{3/2}$. Therefore, they can be mixings of these states. There is information on the mixing angles, obtained from the description of the resonance masses within the quark model with QCD-inspired interquark forces [38] and from the experimental data on the decay widths of the resonances in the πN channel [39]. The results of Ref. [39] are based on the early data. Using recent data [42], we have revised the values of the mixing angles extracted from the πN widths of the resonances. In our calculations of the electroexcitation amplitudes for the $N(1535)\frac{1}{2}^-$, $N(1650)\frac{1}{2}^-$, $N(1520)\frac{3}{2}^-$, and $N(1700)\frac{3}{2}^-$, we have used two sets of mixing angles: one obtained from the description of the mass in Ref. [38] and the other found in the present work from the πN widths of the resonances. The calculated amplitudes for the electroexcitation of the states $^48_{1/2}$ and $^48_{3/2}$ turned out significantly smaller than the amplitudes for the states $^28_{1/2}$ and $^28_{3/2}$. As a result, the mixings have small effects on the electroexcitation amplitudes for the $N(1535)\frac{1}{2}^-$ and $N(1520)\frac{3}{2}^-$, but play a significant role for the $N(1650)\frac{1}{2}^-$ and $N(1700)\frac{3}{2}^-$ resonances.

The approximation of the single quark transition model [43–46] leads to selection rules, which for the resonance $N(1675)\frac{5}{2}^-$ result in the suppression of the amplitudes $A_{1/2}(Q^2)$ and $A_{3/2}(Q^2)$ on the proton. According to our results, relativistic effects violate this suppression weakly, and we expect that experimental values of these amplitudes should be dominated by the meson-baryon contributions. In contrast with protons, the quark core contributions to the electroexcitation amplitudes on the neutron for the $N(1675)\frac{5}{2}^-$ are not suppressed and are predicted to be large.

For the resonances $N(1520)\frac{3}{2}^-$, $N(1535)\frac{1}{2}^-$, and $N(1675)\frac{5}{2}^-$, data on the electroexcitation amplitudes on the proton are available in a wide range of Q^2. This allowed us to present the expected meson-baryon contributions to these amplitudes at $Q^2 < 2 - 3$ GeV^2 inferred from the difference of the LF RQM predictions and the data. The correspondence between these contributions and the meson cloud contributions obtained within the EBAC/Argonne-Osaka coupled-channels analyses [13, 49–52] is discussed in Section IV D.
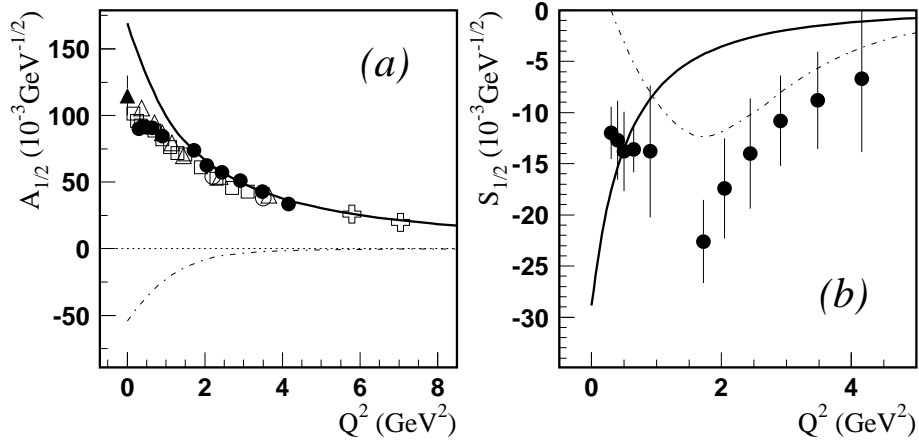
FIG. 1: The $\gamma^* p \to N(1535)\frac{1}{2}^-$ transition helicity amplitudes. The solid curves are the LF RQM predictions; the weight factors for the $3q$ contributions to the nucleon and resonance are taken into account according to (50) and (53) with $c_{N^*} = 0.84$ and 0.94 for the mixing angles $\theta_S = -16.6°$ and $-32°$, respectively, (see (46) and (47)). The thin dashed-dotted curves present the inferred meson-baryon contributions (see Sec. IV D). Solid circles are the amplitudes extracted from CLAS pion electroproduction data [1]. The open triangles [19] and open boxes [20] are the amplitudes extracted from the JLab/Hall B η electroproduction data; the open circles [21] and open crosses [22] are the amplitudes extracted from the JLab/Hall C η electroproduction data; the full triangle at $Q^2 = 0$ is the RPP estimate [42].
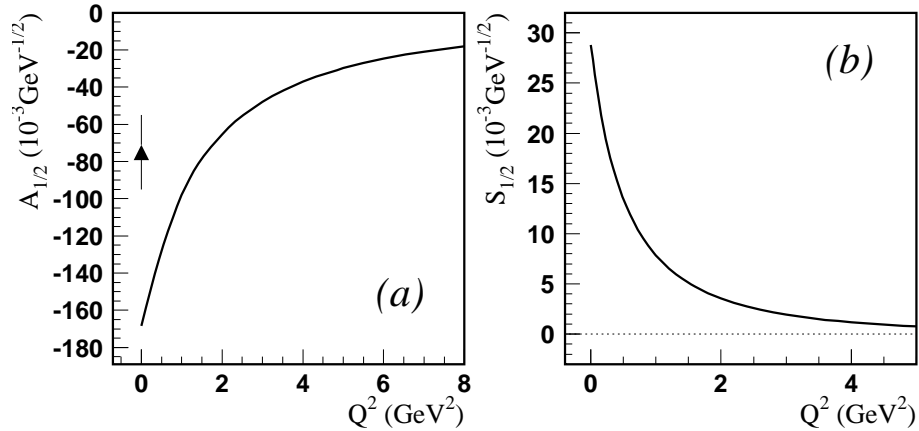
FIG. 2: The $\gamma^* n \to N(1535)\frac{1}{2}^-$ transition helicity amplitudes. The legend for the solid curves is as for Fig. 1. The full triangle at $Q^2 = 0$ is the RPP estimate [42].
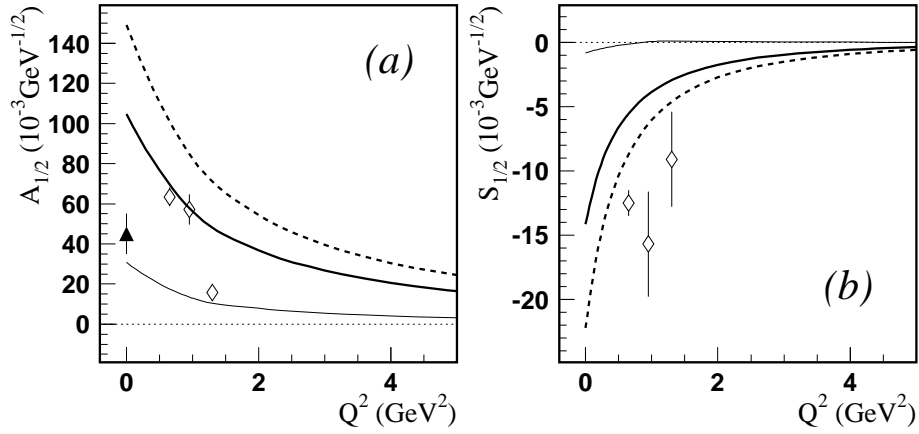
FIG. 3: The $\gamma^* p \to N(1650)\frac{1}{2}^-$ transition helicity amplitudes. The LF RQM predictions are shown by thin and thick solid lines for the mixing angles $\theta_S = 0°$ and $-16.6°$, respectively, and by thick dashed lines for $\theta_S = -32°$ (see (46) and (47)). The full triangle at $Q^2 = 0$ is the RPP estimate [42]; open rhombuses are the amplitudes extracted from CLAS 2π electroproduction data [23].
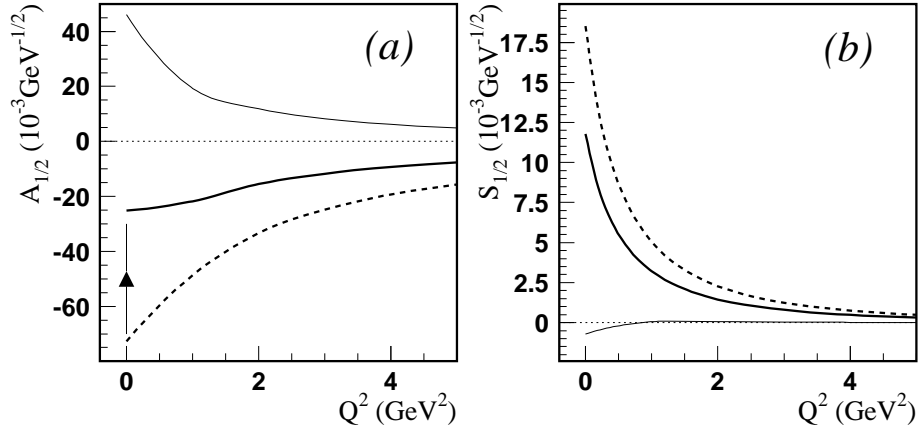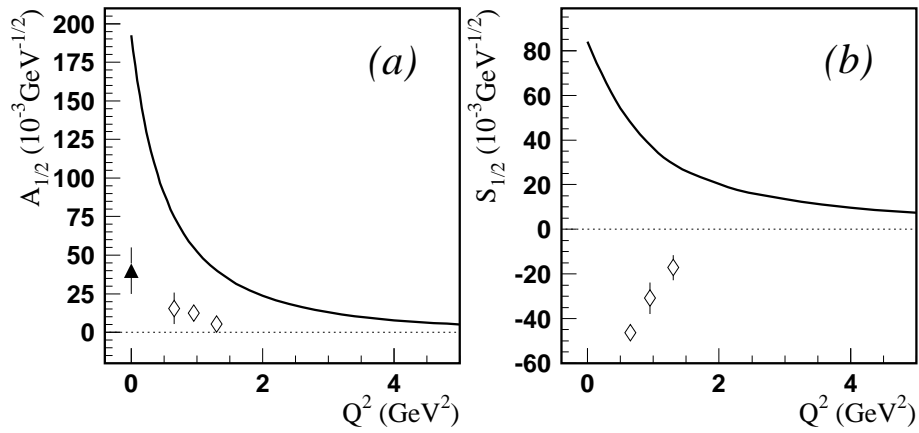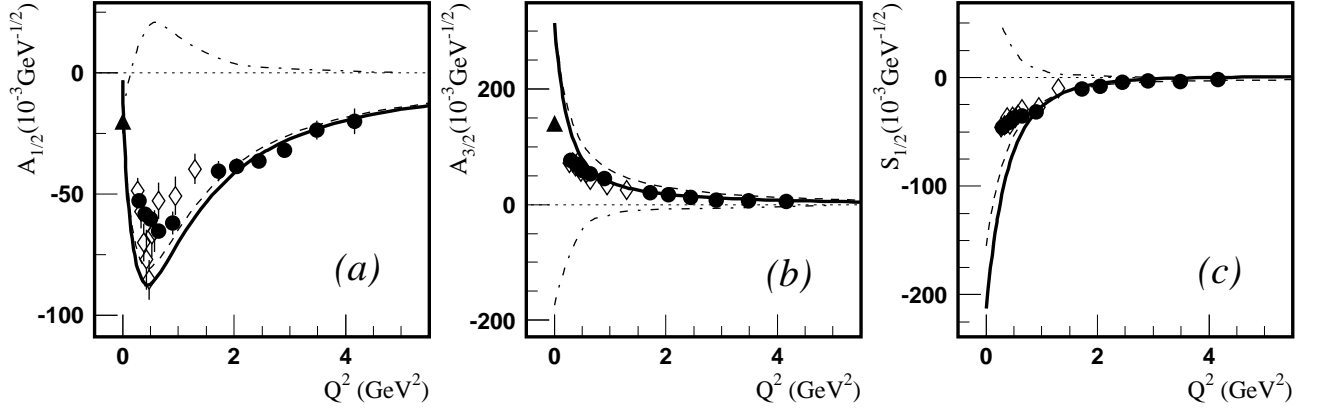

FIG. 4: The $\gamma^* n \to N(1650)\frac{1}{2}^-$ transition helicity amplitudes. The legend for the lines is as for Fig. 3. The full triangle at $Q^2 = 0$ is the RPP estimate [42].

FIG. 5: The $\gamma^* p \to \Delta(1620)\frac{1}{2}^-$ transition helicity amplitudes. The solid curves are the LF RQM predictions. The full triangle at $Q^2 = 0$ is the RPP estimate [42]; open rhombuses are the amplitudes extracted from CLAS 2π electroproduction data [24].

FIG. 6: The $\gamma^* p \to N(1520)\frac{3}{2}^-$ transition helicity amplitudes. The solid curves are the LF RQM predictions; the weight factors for the $3q$ contributions to the nucleon and resonance are taken into account according to (50) and (53) with $c_{N^*} = 0.92$ and 0.94, respectively, for the mixing angles $\theta_D = 6.3°$ and $11.5°$ (see (46) and (47)). The thin dashed curves present our results obtained with $G_3(Q^2) = 0$ (see Sec. IV C). The thin dashed-dotted curves present the inferred meson-baryon contributions (see Sec. IV D). Solid circles are the amplitudes extracted from CLAS pion electroproduction data [1]; open rhombuses are the amplitudes extracted from CLAS 2π electroproduction data [23–25]. The full triangles at $Q^2 = 0$ are the RPP estimates [42].
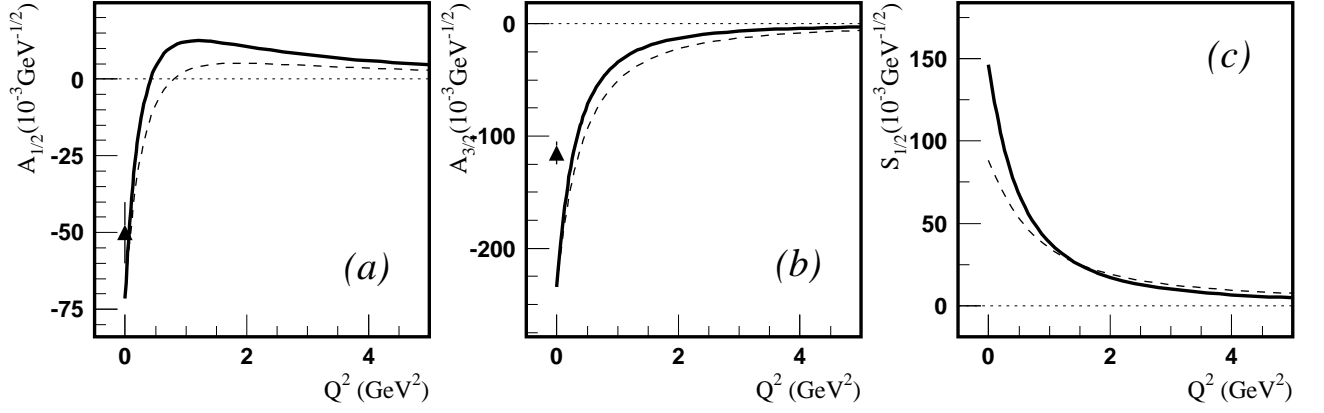

FIG. 7: The $\gamma^* n \to N(1520)\frac{3}{2}^-$ transition helicity amplitudes. The legend for the solid and dashed curves is as for Fig. 6. The full triangles at $Q^2 = 0$ are the RPP estimate [42].
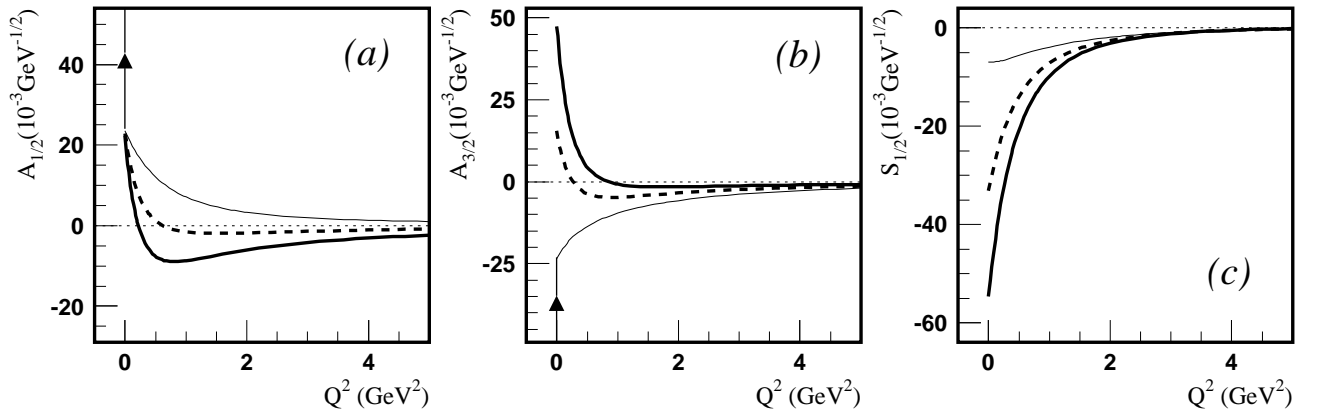

FIG. 8: The $\gamma^* p \to N(1700)\frac{3}{2}^-$ transition helicity amplitudes. The LF RQM predictions are shown by the thin and thick solid lines for the mixing angles $\theta_S = 0$ and $11.5°$, respectively, and by thick dashed lines for $\theta_S = 6.3°$ (see (46) and (47)). The full triangles at $Q^2 = 0$ are the RPP estimates [42].
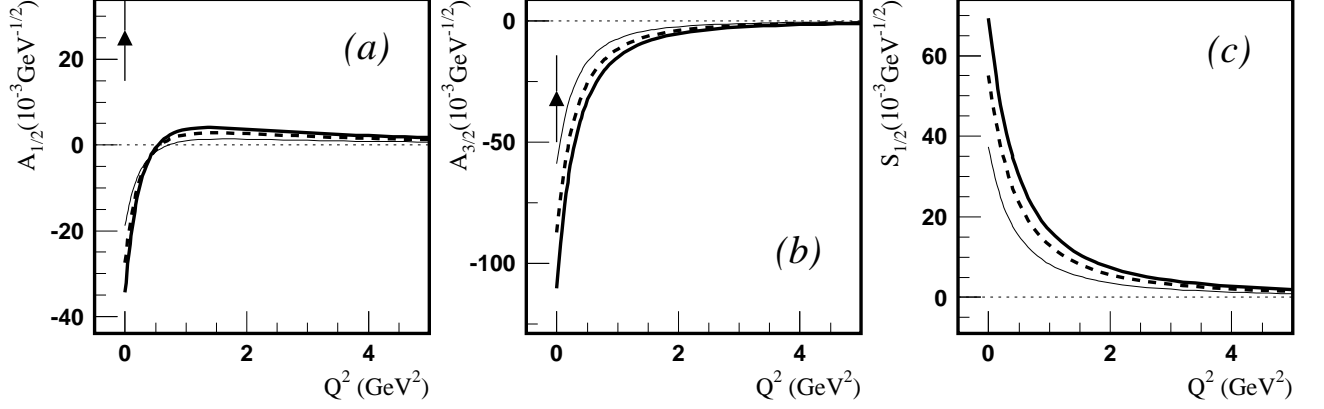
FIG. 9: The $\gamma^* n \to N(1700)\frac{3}{2}^-$ transition helicity amplitudes. The legend for the lines and data is as for Fig. 8.
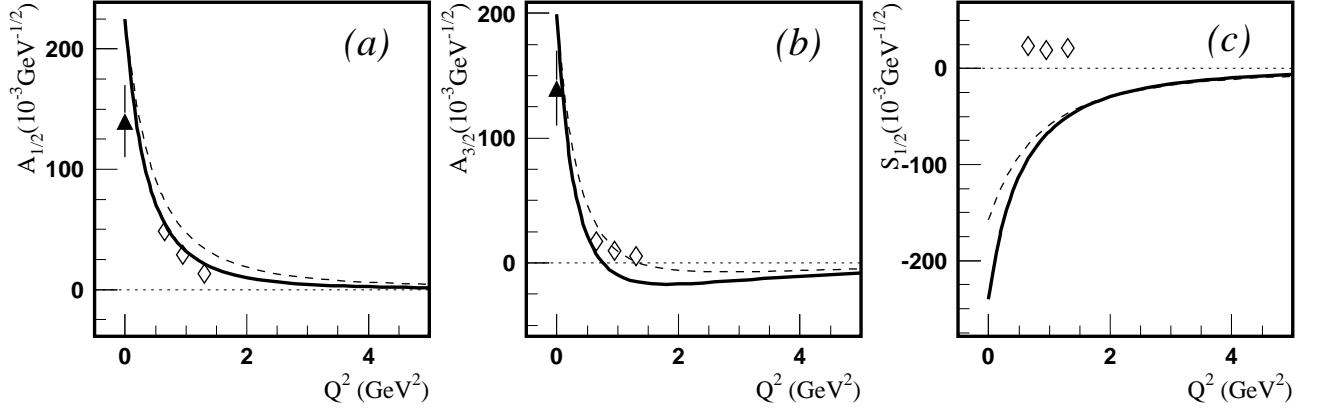

FIG. 10: The $\gamma^* p \to \Delta(1700)\frac{3}{2}^-$ transition helicity amplitudes. The solid curves are the LF RQM predictions. The legend for the thin dashed curves is as for Fig. 6. The full triangles at $Q^2 = 0$ are the RPP estimates [42]; open rhombuses are the amplitudes extracted from CLAS 2π electroproduction data [23].
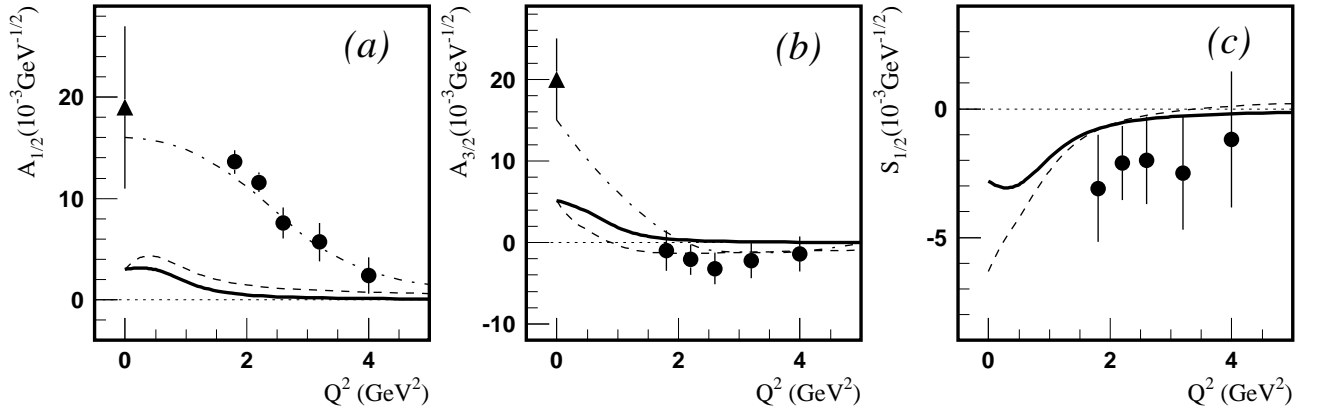

FIG. 11: The $\gamma^* p \to N(1675)\frac{5}{2}^-$ transition helicity amplitudes. The solid curves are the LF RQM predictions. The legend for the thin dashed and dashed-dotted curves is as for Fig. 6. The full triangles at $Q^2 = 0$ are the RPP estimates [42]; the solid circles are the amplitudes extracted from CLAS π electroproduction data [17].
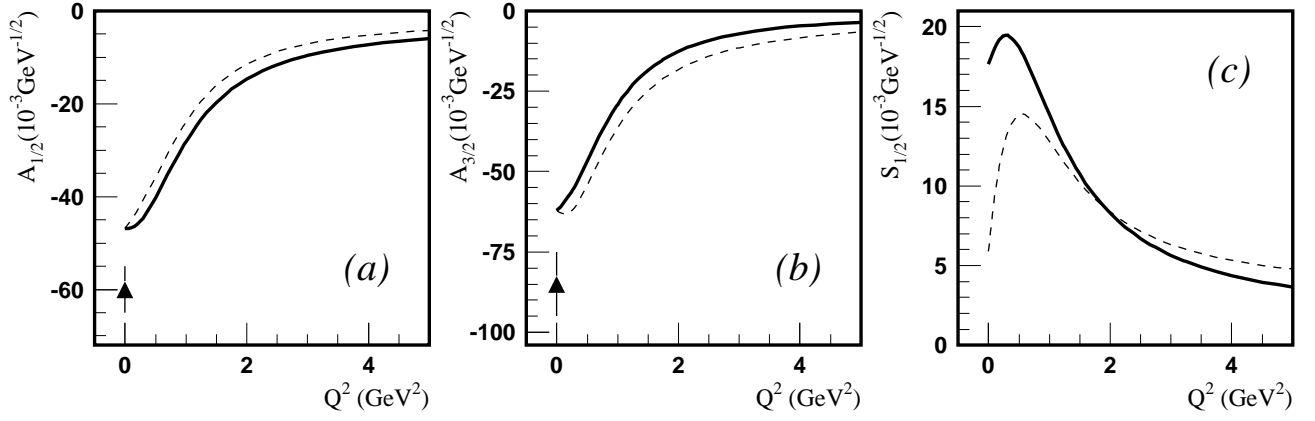
FIG. 12: The $\gamma^* n \to N(1675)\frac{5}{2}^-$ transition helicity amplitudes. The solid curves are the LF RQM predictions. The legend for the thin dashed curves is as for Fig. 6. The full triangles at $Q^2 = 0$ are the RPP estimates [42].

[1] I. G. Aznauryan *et al. (CLAS Collaboration)*, Phys. Rev. C **80**, 055203 (2009).

[2] S. Capstick and B. D. Keister, Phys. Rev. D **51**, 3598 (1995).

[3] I. G. Aznauryan, Phys. Rev. C **76**, 025212 (2007).

[4] S. Stave *et al.*, Eur. Phys. J. A **30**, 471 (2006); Phys. Rev. C **78**, 025209 (2008).

[5] N.F. Sparveris *et al.*, Phys. Rev. Lett. **94**, 022003 (2005); Phys. Lett. B **651**, 102 (2007).

[6] C. Mertz *et al.*, Phys. Rev. Lett. **86**, 2963 (2001).

[7] C. Kunz *et al.*, Phys. Lett. B **564**, 21 (2003).

[8] V.V. Frolov *et al.*, Phys. Rev. Lett. **82**, 45 (1999).

[9] A.N. Villano *et al.*, Phys. Rev. C **80**, 035203 (2009).

[10] J. J. Kelly *et al.*, Phys. Rev. Lett. **95**, 102001 (2005); Phys. Rev. C **75**, 025201 (2007).

[11] T. Sato and T.-S. H. Lee, Phys. Rev. C **63**, 055201 (2001).

[12] V. D. Burkert and T.-S. H. Lee, Int. J. Mod. Phys. E **13**, 1035 (2004).

[13] B. Juliá-Díaz, T.-S. H. Lee, A. Matsuyama, T. Sato, and L. C. Smith, Phys. Rev. C **77**, 045205 (2008).

[14] B. Juliá-Díaz, D. O. Riska, and F. Coester, Phys. Rev. C **69**, 035212 (2004).

[15] I. G. Aznauryan and V. D. Burkert, Phys. Rev. C **92**, 035211 (2015).

[16] I. G. Aznauryan and V. D. Burkert, arXiv:1603.06692,2015.

[17] K. Park *et al. (CLAS Collaboration)*, Phys. Rev. C **91**, 045203 (2015).

[18] I. G. Aznauryan and V. D. Burkert, Phys. Rev. C **92**, 015203 (2015).

[19] R. Thompson *et al.*, CLAS Collaboration, Phys. Rev. Lett. **86**, 1702 (2001).

[20] H. Denizli *et al.*, CLAS Collaboration, Phys. Rev. C **76**, 015204 (2007).

[21] C.S. Armstrong *et al.*, Phys. Rev. D **60**, 052004 (2009).

[22] M.M. Dalton *et al.*, Phys. Rev. C **80**, 015205 (2009).

[23] V.I. Mokeev and I.G. Aznauryan, Int. J. of Modern Phys., Conf. Series, **26**, 1460080 (2014).

[24] V.I. Mokeev *et al.*, arXiv:1509.054650 [nucl-ex].

[25] V.I. Mokeev *et al.*, CLAS Collaboration, Phys. Rev. C **86**, 035203 (2012).

[26] K. Park *et al.*, CLAS Collaboration, Phys. Rev. C **77**, 015208 (2008).

[27] I. G. Aznauryan and V. D. Burkert, Phys. Rev. C **85**, 055202 (2012).

[28] S. D. Drell and T. M. Yan, Phys. Rev. Lett. **24**, 181 (1970).

[29] V. B. Berestetskii and M. V. Terent'ev, Sov. J. Nucl. Phys. **24**, 1044 (1976); **25**, 347 (1977).

[30] S. J. Brodsky and S. D. Drell, Phys. Rev. D **22**, 2236 (1980).

[31] L. A. Kondratyuk and M. V. Terent'ev, Yad. Fiz., **31**, 1087 (1980).

[32] I. G. Aznauryan, A. S. Bagdasaryan, and N. L. Ter-Isaakyan, Phys. Lett. B **112**, 393 (1982); Yad. Fiz. **36**, 1278 (1982).

[33] B. D. Keister and W. N. Polizou, Adv. Nucl. Phys. **20**, 225 (1991).

[34] H. J. Melosh, Phys. Rev. D **9**, 1095 (1974).

[35] R. Koniuk and N. Isgur, Phys. Rev. D **21**, 1868 (1980).

[36] I. G. Aznauryan, V. D. Burkert, Prog. Part. Nucl. Phys. **67**, 1 (2012).

[37] R.C.E. Devenish, T.S. Eisenschitz, and J.G. Körner, Phys. Rev. D **14**, 3063 (1976).

[38] N. Isgur and G. Karl, Phys. Rev. D **18**, 4187 (1978).

[39] A. J. G. Hey, R. J. Litchfield, and R. J. Cashmore, Nucl. Phys. B **95**, 516 (1975).

[40] I. G. Aznauryan and A. S. Bagdasaryan, Yad. Fiz. **41**, 249 (1985).

[41] F. J. Gilman, M. Kugler, and S. Meshkov, Phys. Rev. D **9**, 715 (1974).

[42] C. Patrignani *et al. (Particle Data Group)*, Chinese Physics C **40**, 100001 (2016).

[43] A.J.G. Hey and J. Weyers, Phys. Lett. B **48**, 69 (1974).

[44] J. Babcock and J.L. Rosner, Ann. Phys. (N.Y.) **96**, 191 (1976) .

[45] W.N. Cottingham and I.H. Dunbar, Z. Phys. C **2**, 41 (1979).

[46] V.D. Burkert *et al.*, Phys. Rev. C **67**, 035204 (2003).

[47] E. Santopinto and M. M. Giannini, Phys. Rev. C **86**, 065202 (2012).

[48] B. D. Keister, Phys. Rev. D **49**, 1500 (1994).

[49] B. Juliá-Díaz, H. Kamano, T.-S. H. Lee, A. Matsuyama, T. Sato, and N. Suzuki, Phys. Rev. C **80**, 025207 (2009).

[50] H. Kamano, S. X. Nakamura, T.-S. H. Lee, and T. Sato, Phys. Rev. C **94**, 015201 (2016).

[51] H. Kamano, talk presented on INT workshop "Spectrum and Structure of Excited Nucleons from Exclusive Electroproduction", Seattle, USA, November, 2016.

[52] T. Sato, talk presented on INT workshop "Spectrum and Structure of Excited Nucleons from Exclusive Electroproduction", Seattle, USA, November, 2016.